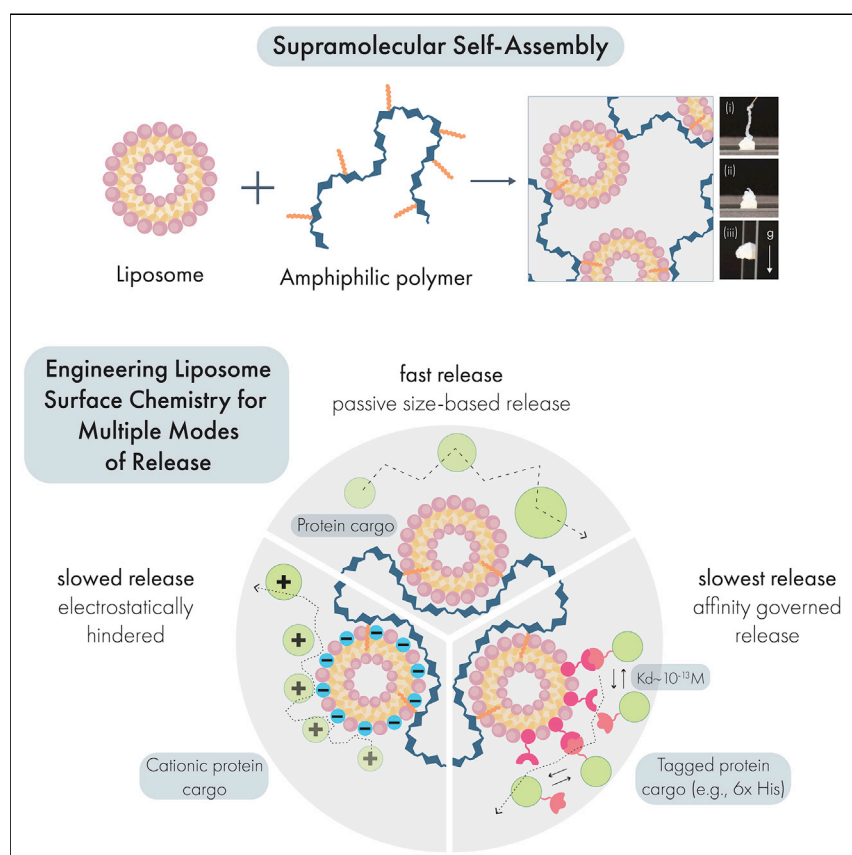# Matter

Article

Injectable liposome-based supramolecular hydrogels for the programmable release of multiple protein drugs

Liposome nanocomposite hydrogels (LNHs) are developed through simple mixing of liposomes and modified cellulose polymers. These hydrogels exhibit tunable mechanical properties and are easily injected through standard syringe needles. Engineering the liposome surface chemistry enabled the programmable, affinity-based release of proteins independent of cargo size. LNHs can act as a depot to synchronously release diverse therapeutics *in vivo*. We envision use of LNHs for biomedical applications requiring tunable release of multiple protein drugs.

Santiago Correa, Abigail K. Grosskopf, John H. Klich, Hector Lopez Hernandez, Eric A. Appel

eappel@stanford.edu

Highlights

Liposomal nanocomposite hydrogels (LNHs) are injectable and easily fabricated

LNH mechanical properties are tuned by the amount of liposome within the formulation

Engineering liposome surface chemistry enables orthogonal modes of protein release

LNHs act as a depot to simultaneously deliver different size proteins *in vivo*

Demonstrate
Proof-of-concept of performance with intended application/response

4

Matter

CellPress

Article

Injectable liposome-based supramolecular hydrogels for the programmable release of multiple protein drugs

Santiago Correa,[1,7] Abigail K. Grosskopf,[2,7] John H. Klich,[3] Hector Lopez Hernandez,[1] and Eric A. Appel[1,3,4,5,6,8,*]

SUMMARY

Directing biological functions is at the heart of next-generation biomedical initiatives in tissue and immuno-engineering. However, the ambitious goal of engineering complex biological networks requires the ability to precisely perturb specific signaling pathways at distinct times and places. Using lipid nanotechnology and the principles of supramolecular self-assembly, we developed an injectable liposomal nanocomposite hydrogel platform to precisely control the release of multiple protein drugs. By integrating modular lipid nanotechnology into a hydrogel, we introduced multiple mechanisms of release based on liposome surface chemistry. To validate the utility of this system for multi-protein delivery, we demonstrated synchronized, sustained, and localized release of immunoglobulin G (IgG) antibody and interleukin-12 (IL-12) cytokine _in vivo_, despite the significant size differences between these two proteins. Overall, liposomal hydrogels are a highly modular platform technology with the ability to mediate orthogonal modes of protein release and the potential to precisely coordinate biological cues both _in vitro_ and _in vivo_.

INTRODUCTION

Protein drugs are essential tools for engineering biological systems to improve human health. Challenging biomedical applications, such as tissue regeneration and wound healing, often rely on diverse growth factors and cytokines.[1,2] Likewise, immunotherapy relies heavily on antibodies, engineered proteins, cytokines, and chemokines to activate or dampen the immune system (e.g., for cancer or autoimmune disorders, respectively).[3] While tissue regeneration, wound healing, and immuno-engineering pursue different biological outcomes, they share a similar challenge—to manipulate complex biological networks. The capacity to successfully rewire these networks rests on the ability to perturb multiple dynamic signaling pathways at specific times[4] and within specific tissues (e.g., diseased tissues or specific lymphoid organs) to achieve desired therapeutic outcomes.[5] Indeed, disruption of these networks outside of the appropriate time frame or outside of the target tissues can lead to serious side effects.[5,6] Taken together, technology that can precisely coordinate the release kinetics of diverse protein drugs in specific locations is critical for the controlled modulation of biological systems.

Nanomedicine and injectable hydrogel technologies seek to provide precise spatiotemporal control over drug delivery.[6–8] In terms of spatial control, nanoparticle drug carriers seek to preferentially accumulate in target tissues after systemic

Progress and potential

Many technologies developed for controlled release of soluble cargo rely on passive diffusion, which renders release kinetics primarily dependent on the cargo's size and limits the ability to coordinate the release of multiple cargo. Nevertheless, precisely controlled multi-drug delivery is critical for initiatives in tissue and immuno-engineering that require precise control over the timing, location, and dosing of multiple signaling molecules. Here, we report the development of liposomal nanocomposite hydrogels (LNHs) that are syringe injectable and enable the programmable release of protein cargo. LNHs control cargo release through tunable supramolecular interactions, independent of cargo size and physicochemical properties, to orthogonally tune release behaviors of multiple protein cargo. These modular, scalable, and easily administered hydrogel materials will enable tunable release of diverse therapeutics to develop efficacious treatments to improve human health.

administration, but besides filtration organs like the liver and spleen, their ability to target to specific tissues is limited.[9–11] In terms of scheduled multi-drug release, nanomedicine has been successful in staging the release of different classes of drugs (e.g., hydrophilic versus hydrophobic small molecules, nucleic acids, and proteins), but staged delivery of proteins remains a challenge.[8,12] Meanwhile, the emergence of injectable hydrogels has provided a significant improvement for minimally invasive localized therapy,[13–22] but scheduled multi-drug release from these systems is often limited to strategies that leverage size-governed (e.g., smaller drugs first) or solubility-governed (e.g., most soluble drugs first) release mechanisms.[7,23] Overall, there remains no minimally invasive delivery technology that can tune the relative release rates of multiple protein drugs *in vivo*.

To address this technology gap, we developed a supramolecular hydrogel platform constructed directly from dodecyl-modified hydroxypropylmethylcellulose (HPMC-C$_{12}$) and liposomal nanoparticle building blocks (Scheme 1A). This hydrogel material was inspired by previously developed polymer-nanoparticle hydrogels based on other solid nanoparticles.[24–26] By integrating liposomes directly into the hydrogel network, this system possesses several distinct drug compartments useful for multi-protein delivery. Moreover, as an injectable hydrogel, this system allows for highly localized delivery of cargo, which is not possible with free liposomal carriers.

In this report, we provide a comprehensive assessment of how the clinically relevant rheological properties of these liposomal nanocomposite hydrogels (LNHs) are influenced by critical formulation parameters (e.g., liposome size and concentration). In general, the mechanical properties of the LNHs are readily tuned by liposome concentration and to a lesser extent size, and they are robust to changes in liposome composition. We performed preclinical toxicology studies in immunocompetent mice to determine the biocompatibility of LNHs, where we observed a steady erosion of the hydrogel over time with no signs of toxicity. Finally, we determined the ability of LNHs to stage the release of protein drugs through orthogonal passive, electrostatic, and affinity-based release mechanisms (Scheme 1B). We validated the utility of our orthogonal release approach by using LNHs to synchronize the sustained local delivery of immunoglobulin G (IgG) antibody and interleukin-12 (IL-12) cytokines *in vivo*, despite the significant size difference between these two protein drugs. Overall, LNHs leverage the impressive capabilities of lipid nanotechnology to generate a shear-thinning and self-healing biomaterial platform capable of simultaneously accommodating numerous mechanisms of protein drug release. We anticipate this platform will provide a readily generalizable approach for the localized staged release of protein drugs, with implications for the fields of immunotherapy and regenerative medicine.

RESULTS AND DISCUSSION

Liposomes spontaneously form injectable hydrogels when mixed with hydrophobically modified biopolymers

To stably incorporate liposomal nanoparticles into a supramolecular hydrogel network, we exploited the ability for hydrophobic carbon chains to post-insert into lipid membranes.[27] To this end, we modified high-molecular-weight HPMC-C$_{12}$ with fatty dodecyl side chains to introduce a molecular motif capable of post-insertion. In addition to HPMC, other cellulosic polymers and hyaluronic acid have functioned similarly in other polymer-nanoparticle-based materials.[24,28] Initially, we prepared liposomal nanoparticles composed of 1,2-dimyristoyl-*sn*-glycero-3-phosphocholine (DMPC) (zwitterionic head group), 1,2-dimyristoyl-*sn*-glycero-3-phospho-(1′-rac-glycerol) (DMPG) (anionic head group), and cholesterol at a

[1]Department of Materials Science & Engineering, Stanford University, Stanford, CA 94305, USA

[2]Department of Chemical Engineering, Stanford University, Stanford, CA 94305, USA

[3]Department of Bioengineering, Stanford University, Stanford, CA 94305, USA

[4]ChEM-H Institute, Stanford University, Stanford, CA 94305, USA

[5]Department of Pediatrics – Endocrinology, Stanford University School of Medicine, Stanford, CA 94305, USA

[6]Woods Institute for the Environment, Stanford University, Stanford, CA 94305, USA

[7]These authors contributed equally

[8]Lead contact

*Correspondence: eappel@stanford.edu

https://doi.org/10.1016/j.matt.2022.03.001

CellPress
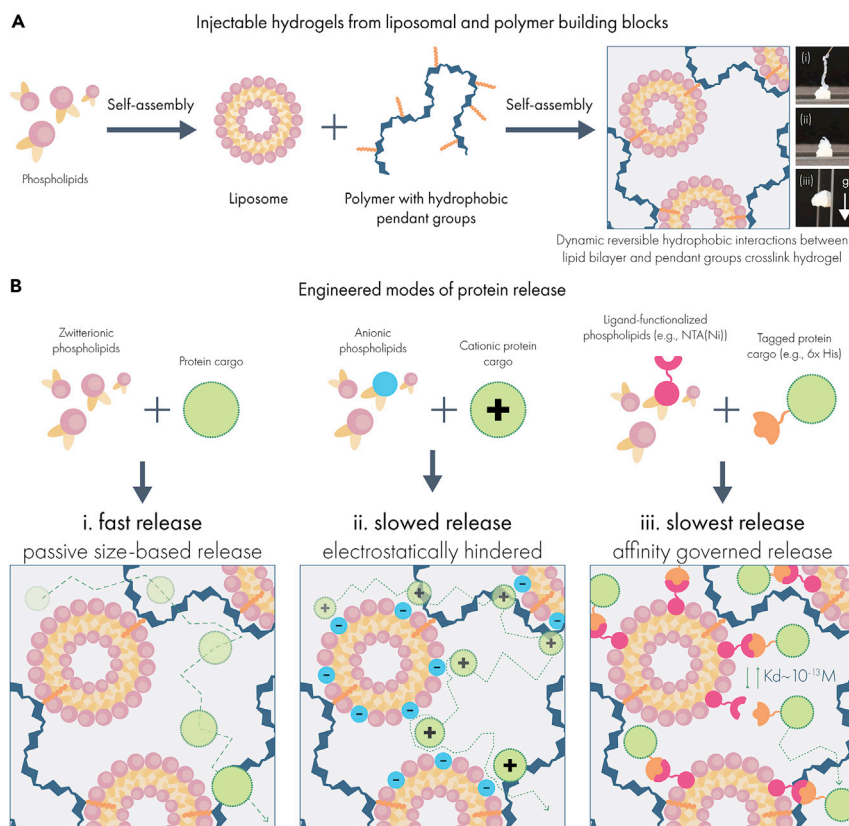
Scheme 1. Forming injectable hydrogels for multi-modal protein drug delivery from liposomal building blocks

(A) Liposomes self-assemble from phospholipids to form nanoparticles featuring a hydrophobic compartment within the lipid bilayer. When liposomes are mixed with dodecyl-modified hydroxypropyl methylcellulose (HPMC-C_{12}), the hydrophobic dodecyl pendants insert into the lipid membrane, generating a crosslinked hydrogel network.

(B) Drug delivery capabilities are tuned by incorporating functional phospholipids into the liposomal building blocks, which establish interactions with protein cargo in the hydrogel. These include (i) zwitterionic liposomes that minimize interactions with cargo and mediate release by size-based diffusion, (ii) charge-carrying liposomes that engage with proteins exhibiting an opposite net charge, and (iii) ligand-functionalized liposomes that establish affinity-mediated release of specific protein cargo.

9:1:2 M ratio using the thin-film rehydration and extrusion method.[29] This formulation was chosen for its previously reported utility for drug delivery.[29] Following extrusion through 50-nm polycarbonate filters, liposomes exhibited a monodisperse average hydrodynamic size of 90.4 nm and a polydispersity index (PDI) of 0.1, indicating uniform nanoparticle preparation. Physical mixing of HPMC-C_{12} and liposome solutions led to the generation of a pearlescent supramolecular hydrogel comprising 2 wt % polymer and 10 wt % liposome, which we denote as 2P-10L. An interparticle spacing calculation reveals that these liposomes are not touching at this concentration (interparticle spacing of 17 nm), and the volume fraction is far below the packing fraction of monodisperse spheres (volume fraction of 0.25).[30]

Dynamic oscillatory shear rheology of the resulting 2P-10L hydrogel revealed robust solid-like characteristics (e.g., G' greater than G'') over the entire range of frequencies evaluated (Figure 1A). The robust mechanical properties of these LNHs, with no observable crossover of G' and G'' in the low-frequency-oscillation regime,
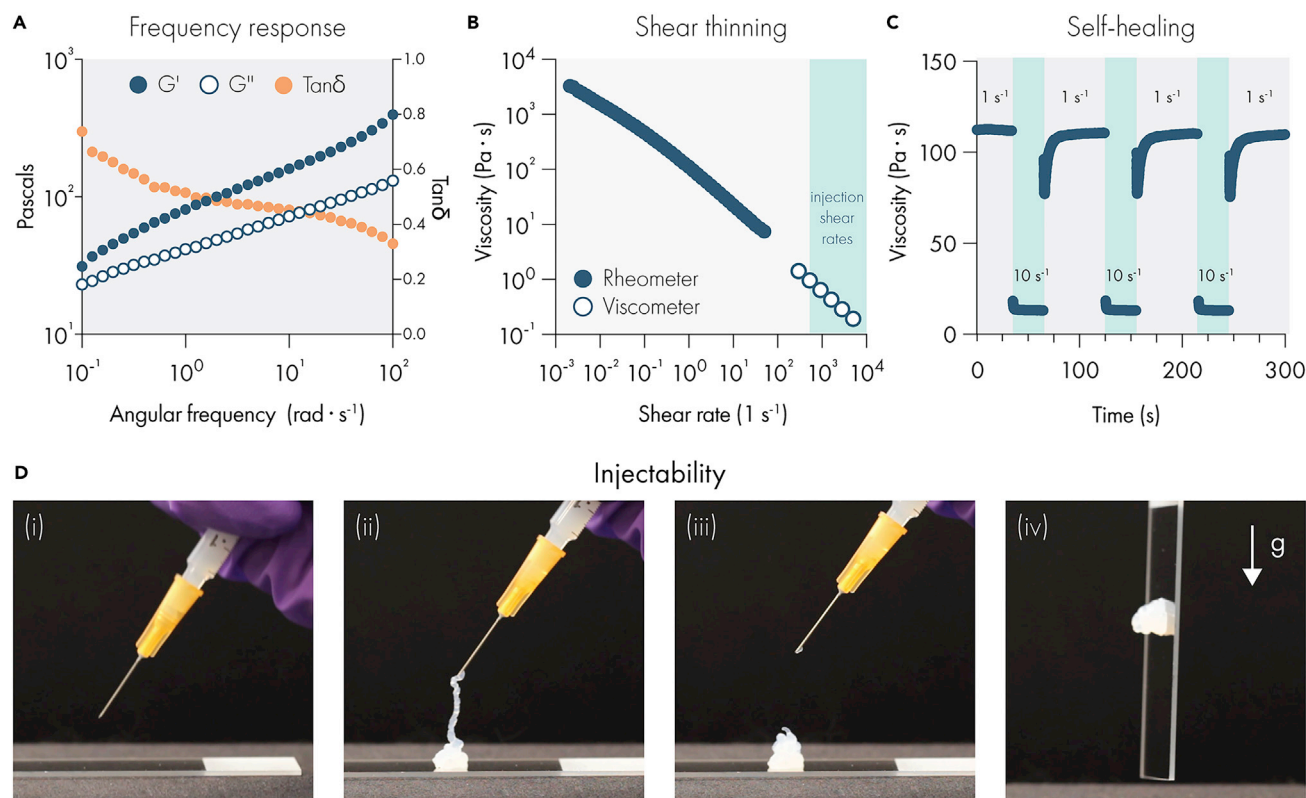
Figure 1. Liposomal hydrogels exhibit shear thinning and self-healing mechanical properties that enable injection through needles

(A) Dynamic oscillatory shear rheology of liposomal hydrogels (2 wt % HPMC-C_{12}; 10 wt % 50 nm extruded liposome) indicates the storage modulus (G′) is greater than the loss modulus (G″) over a broad range of frequencies, demonstrating robust solid-like properties.

(B) Steady shear rheology measurements (filled circles) and viscometer measurements (empty circles) indicate that the viscosity of liposomal hydrogels steadily decreases by roughly four orders of magnitude as shear rates approach injection conditions.

(C) Step-shear rheology measurements demonstrate that liposomal hydrogels can repeatedly regain their original viscosity after exposure to high shear conditions.

(D) Representative photographs of liposomal hydrogels injected through a 26G needle fitted onto a 1-mL syringe.

indicates successful hydrogel formation and sets these materials apart from previously reported liposome-based hydrogels that exhibit a measurable crossover and may flow over long timescales.[31] However, it is difficult to fully compare these results with prior systems due to a lack of comprehensive mechanical characterization of these systems in the literature. In contrast, when liposomes were mixed with unmodified HPMC, no hydrogel was formed and rheological characterization revealed the mixture exhibited liquid-like properties (e.g., G″ greater than G′) over a broad range of frequencies (Figure S1B). Likewise, solutions of 2 wt % HPMC-C_{12} fail to form robust hydrogels in the absence of liposomes (Figure S1C). Overall, these data strongly indicate that LNHs are formed from multivalent and dynamic polymer-particle crosslinking interactions between the liposomal and polymer building blocks that require the presence of a hydrophobic molecular motif on the cellulosic polymer component.

We then set out to determine whether LNHs exhibited necessary mechanical properties for the development of a clinically relevant drug delivery platform.[32] First, we evaluated whether these materials possess shear-thinning and self-healing properties, which would allow them to serve as injectable depots of therapeutic compounds. To test this, we performed steady shear rheology and viscometry to

CellPress

evaluate how LNH viscosity changes under high shear conditions, representative of the shear forces in a syringe needle (Figure 1B). We observed that LNH viscosity drops approximately four orders of magnitude as shear rates increase to levels that simulate syringe-needle injection. A power law fit to the flow sweep gives a consistency index K of 119.8 and a shear thinning index n of 0.27. Following the guidelines given by Lopez et al.,[32] for a 26G needle and human forces for injection, we find this material is well within the injectable range for translational use (Figure S1D). The steep decrease in the viscosity suggests that the internal structure of the LNH network is disrupted during high-shear conditions, which would require the structure to spontaneously regenerate in order for the LNH to re-solidify after injection.[32] To determine the ability for LNHs to self-heal, we conducted step-shear experiments where the material undergoes multiple cycles of high- and low-shear conditions (Figure 1C). Rapid self-healing is essential to prevent burst release of protein cargo upon injection.[33] We observed the viscosity of LNHs rapidly and repeatedly restored to original levels once high-shear conditions were suspended. We also observed that LNHs could be easily injected through 1-mL syringes fitted with 26G needles and re-solidify after injection (Figure 1D; Video S1). These data indicate that LNHs are able to dynamically re-assemble the hydrogel network following its disruption, consistent with a supramolecular mechanism of assembly and providing a minimally invasive administration route for drug delivery.

Our next objective was to determine how robust these supramolecular assemblies were to changes in the liposome formulation. Our initial liposomes followed an anionic formulation previously validated for drug delivery,[29] but one of the assets of lipid nanotechnology is the broad parameter space available to tune key properties (e.g., surface chemistry, surface charge, anti-fouling, and melting temperature) through careful selection of the individual phospholipid components. We evaluated how a cationic version of our liposomes (replacing the 1,2-dimyristoyl-*sn*-glycero-3-phosphoglycerol with the cationic phospholipid 1,2-dioleoyl-3-trimethylammonium-propane) behaved when mixed with HPMC-C_{12} and observed that these systems yielded hydrogels with similar rheological properties to our original formulations (Figure S3). Like the hydrogels formed with anionic liposomes, the cationic liposomal hydrogels were solid-like over the same range of frequencies and were both shear thinning and self-healing. Next, we evaluated how a polyethylene glycol (PEG)ylated liposomal formulation behaved in this platform, and we observed overall consistent mechanical properties (Figure S4). This compatibility with diverse liposomal formulations expands the biomedical capabilities of these materials. For example, the ability to incorporate cationic liposomes is promising for the development of injectable materials for gene delivery.[34] Likewise, the anti-fouling capabilities of PEGylated formulations could be leveraged to reduce engagement with the host after injection.[35] Moreover, since most clinically approved liposomal drugs feature PEGylation, this technology could provide a means to locally administer approved liposomal drugs through minimally invasive injections.

Having confirmed that anionic, cationic, and PEGylated liposomes yield consistent hydrogels in our system, we began to evaluate the parameters of cholesterol content and lipid melting temperature (T_m) on the resulting rheological properties of these materials. These properties are often varied to tune drug retention and liposome stability.[36,37] Using our anionic liposome formulation as a starting point, we evaluated hydrogels generated from liposomes composed of 17, 37.5, and 50 mol % cholesterol (Figure S5). Overall, we observed that the modulus of the materials and the shear-thinning behaviors were consistent as cholesterol content was varied. Yet we did observe a difference in the yield strain between high and low cholesterol

formulations, with low-cholesterol liposomal hydrogels exhibiting an ~4-fold higher yield strain. To evaluate whether lipid T_m impacted hydrogel mechanical properties, we evaluated hydrogels generated from low T_m ($-17°C$; dioleoyl tails) and high T_m ($55°C$; distearoyl tails) phospholipids (Figure S6). Despite the significant difference in T_m, these hydrogels exhibited consistent mechanical properties, except for the storage modulus G', which was moderately elevated in the high T_m formulation. Overall, these data provide compelling evidence that liposomal hydrogels are robust to the liposome formulation. This versatility makes this platform broadly attractive for the conversion of any liposome-based nanotechnology into an injectable hydrogel.

Lipid content and liposome size influence rheological properties of liposomal hydrogels

The mechanical properties of conventional hydrogels are tuned by changing the concentration of solids and crosslinkers in the system. Prior work has also established that increasing the crosslinking of the hydrogel leads to increased persistence times and thus protein release timescales *in vivo*.[16,38] Since the liposomal building blocks serve as crosslinkers in our hydrogel system, we set out to determine whether lipid content could tune the mechanical properties of liposomal hydrogels. We found that, as lipid content increased from 1 to 10 wt %, the resulting hydrogels became both stiffer and more solid-like across a broad range of frequencies (Figures 2A, 2B, and S2). For all formulations, no crossover was observed between the G' and G'' across the frequency range examined, indicating robust hydrogel formation across a wide range of lipid contents and timescales. Likewise, amplitude sweeps for each formulation demonstrated very high strains upon yielding and smooth yielding transitions with no brittle fracture. From these data, the modulus of LNH systems (E from 0.3 to 1 kPa) appears to be comparable to the widely used alginate systems (0.2–1.3 kPa).[39] Overall, this range is compatible with a variety of soft tissues[40] and is in a range that has been previously reported to be useful for immuno-engineering applications, such as T cell engineering.[41]

Each formulation yielded a high-quality hydrogel, and we observed consistent yield strain behavior once lipid content was increased beyond 1% (Figures 2C and 2D). To characterize the yielding behavior of these materials more fully, we performed flow sweeps to assess each formulation's yield stress behavior. Both shear-rate-imposed flow sweeps (from high shear rate to low shear rate) and stress sweeps (from low stress to high stress) were performed (Figures 2E and 2F). These data indicated that all formulations exhibit extreme shear-thinning behavior, minimal thixotropy (as shown by the high degree of overlap in our two methods), and significant yield stress values (as indicated by the stress at which the viscosity abruptly decreases in the stress sweep). Overall, the high yield stress values noted for these formulations suggest that these materials are ideal for forming and maintaining subcutaneous drug depots robust to the low but constant stresses imposed by the dermis.

Next, the effect of liposome size on mechanical properties was investigated. As liposome size is increased at a constant mass loading in the hydrogel, there are fewer liposomes per unit volume. This decrease in the number of liposomes leads to greater interparticle spacing[42,43] and reduces the total liposomal surface area with which the cellulose polymers can interact, likely reducing the efficiency of crosslinking interactions. Our data confirm these hypotheses and suggest that increasing liposome size leads to less stiff hydrogels with constant solid-like properties (Figures 3A, 3B, and S2). While stiffness (G') and solid-like properties (tan delta = G''/G') are often correlated, it is fascinating that this modular system exhibits the ability to
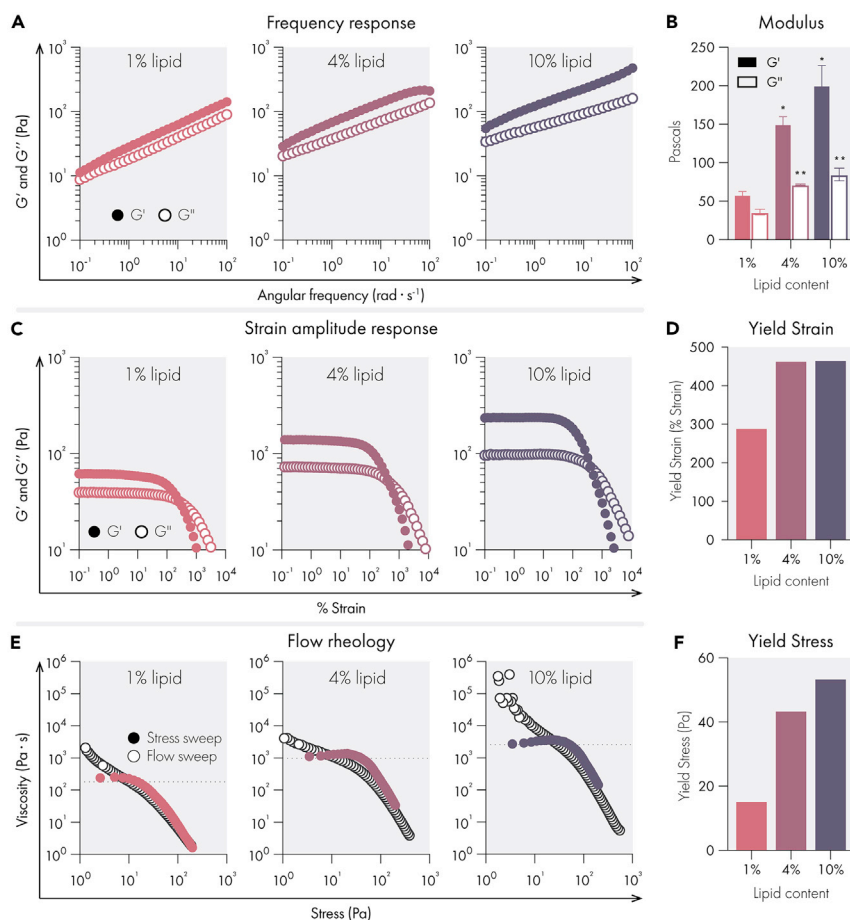
Figure 2. Mechanical properties of liposomal hydrogels are tuned by liposome concentration in the hydrogel

All measurements were performed on hydrogels composed of 1%, 4%, and 10% 50 nm extruded liposome content (by weight). All hydrogel formulations were 2% HPMC-C_{12} by weight.

(A) Oscillatory shear rheology measurements indicate increased liposome content increases G′ and G″.

(B) G′ and G″ values at 10 rads/s; data represent mean and SEM of two replicate batches.

(C) Strain-controlled oscillatory shear rheology.

(D) Yield strain values extracted from strain amplitude response data.

(E) Flow rheology overlay showing low to high stress-sweep behavior (solid circles) and high to low flow sweep (empty circles).

(F) Yield stress values extracted from flow rheology data.

Statistical comparisons were made using a one-way ANOVA, and the false discovery rate (FDR) was controlled at 5% using the Benjamini, Krieger, and Yekutieli method.

independently tune stiffness without changing the solid-like properties. All formulations exhibited high yield strains (>250%; Figures 3C and 3D) and measurable yield stress behavior (Figures 3E and 3F).

Extensional rheology has been found to be highly important during injection. High extensional forces at the flow entrance of the syringe needle have been found to both denature delivered proteins and lead to cell death for cell injections.[44,45] Designing extensible hydrogel materials can both improve injectability and alleviate these issues.[44,46] Extensible materials have also been demonstrated to improve 3D bioprinting fidelity.[47] Upon handling our liposomal hydrogels, we noted both sticky
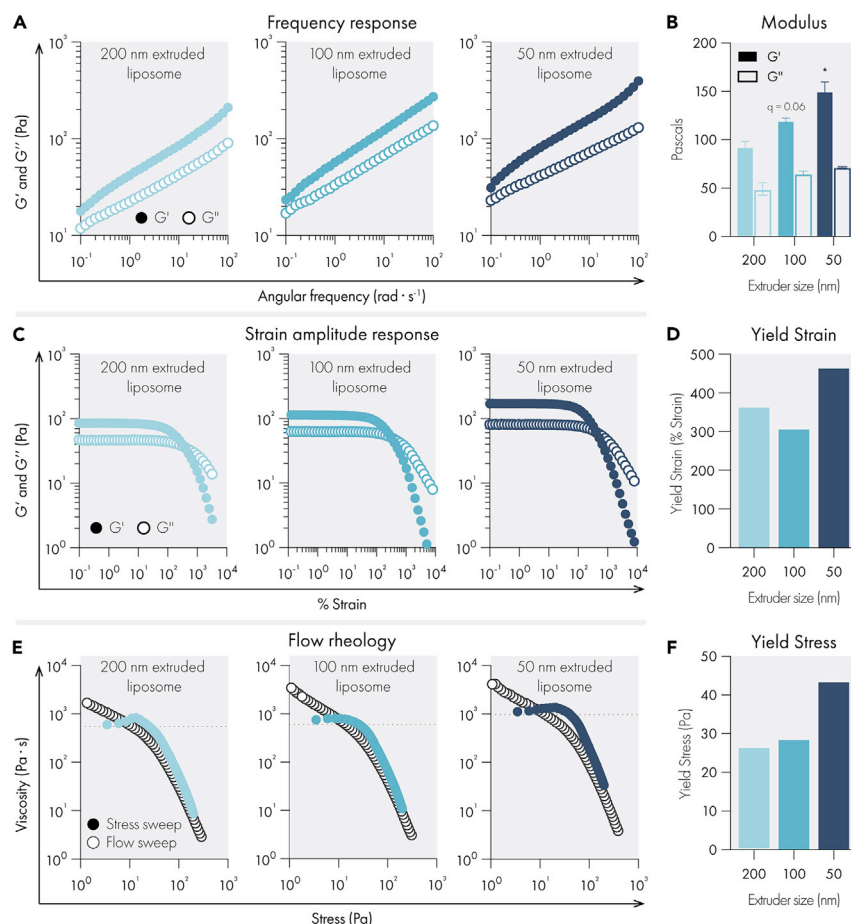
Figure 3. Liposome size impact on rheological properties of liposomal hydrogels

All measurements were performed with hydrogels composed of 2% HPMC-C$_{12}$ and 4% liposome, by weight. Liposomes were extruded through either 200-, 100-, or 50-nm polycarbonate filters.

(A) Representative oscillatory shear rheology.

(B) G′ and G″ at 10 rads/s indicates G′ is influenced by liposome size. Data represent the mean and SEM of two replicate batches.

(C) Representative strain-controlled oscillatory shear rheology.

(D) Yield strain values extracted from the strain amplitude response data.

(E) Representative flow rheology overlay showing low to high stress-ramp behavior (solid circles) and high to low flow sweep (empty circles).

(F) Yield stress values extracted from flow rheology data.

Statistical comparisons were made using a one-way ANOVA, and the FDR was controlled at 5% using the Benjamini, Krieger, and Yekutieli method.

and extensional characteristics. To further investigate these attributes, we performed filament stretching rheology to assess the formulations' strain to break (Figure 4). Notably, we observed extreme extensibility for all formulations across several strain rates that are higher than all other physically crosslinked biomaterials reported to date.[48] Intriguingly, we observed a moderate but significant increase in extensibility with an increase in liposome size (Figure 4D).

Liposomal hydrogels are non-toxic and recruit cell infiltrates in healthy mice

To confirm that liposomal hydrogel technology is suitable for biomedical applications, we conducted toxicological studies in immuno-competent C57BL6 mice. We injected 100-μL doses of liposomal hydrogel (2% HPMC-C$_{12}$ polymer; 4%
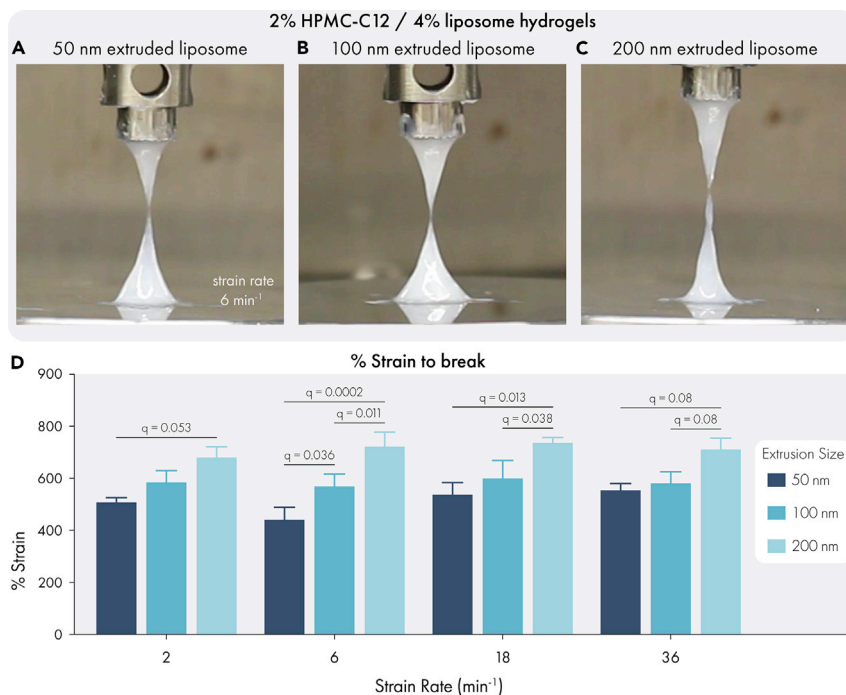
Figure 4. Liposome size influences the extensional properties of liposomal hydrogels

All measurements were performed with hydrogels composed of 2% HPMC-C_{12} and 4% liposome, by weight. Liposomes were extruded through either 200-, 100-, or 50-nm polycarbonate filter.

(A–C) Representative images of filament breakage with hydrogels composed of liposomes extruded through (A) 50-nm, (B) 100-nm, or (C) 200-nm polycarbonate filters.

(D) Quantification of % strain to break for each formulation at a range of strain rates. Data represent mean and SEM of three independent batches.

Statistical comparisons were made using a two-way ANOVA, and the FDR was controlled at 5% using the Benjamini, Krieger, and Yekutieli method.

liposome; 2P-4L) subcutaneously into the hind flank of mice, where we observed the material take on a well-defined spherical shape (Figure 5A). Over the course of the following week, we monitored the mice daily for signs of skin irritation and weight loss or any signs of morbidity, and we also tracked the size of the hydrogel depot using calipers. We did not observe any signs of skin irritation with the 2P-4L formulation (Figures 5B and 5C), and we noted that this formulation slowly dissolved over time until the material was explanted on day 7 (Figure 5D). Caliper measurements of the hydrogel area indicated that the depot was steadily eroding after implantation (Figure 5E), indicating that liposomal hydrogels are cleared without signs of toxicity or inflammation. This observation was further bolstered by the stable body weights of hydrogel-treated mice (Figure 5F), which exhibited consistent weights compared with untreated control animals.

Seven days after hydrogel injection, we collected serum from the mice to evaluate common markers of liver and renal toxicity. We observed that hydrogel-treated mice had comparable aspartate transaminase (AST)/alanine aminotransferase (ALT) ratios and alkaline phosphatase (ALP) levels to untreated control mice (Figures 5H and 5I), which indicates that these hydrogels do not induce acute hepatotoxicity after administration. Similarly, we found that hydrogel-treated and control mice had similar blood urea nitrogen (BUN) and creatinine levels, suggesting that no short-term renal toxicity occurs after injection with liposomal hydrogels. Overall, these data indicate that liposomal hydrogels do not pose a risk of acute liver or kidney damage.
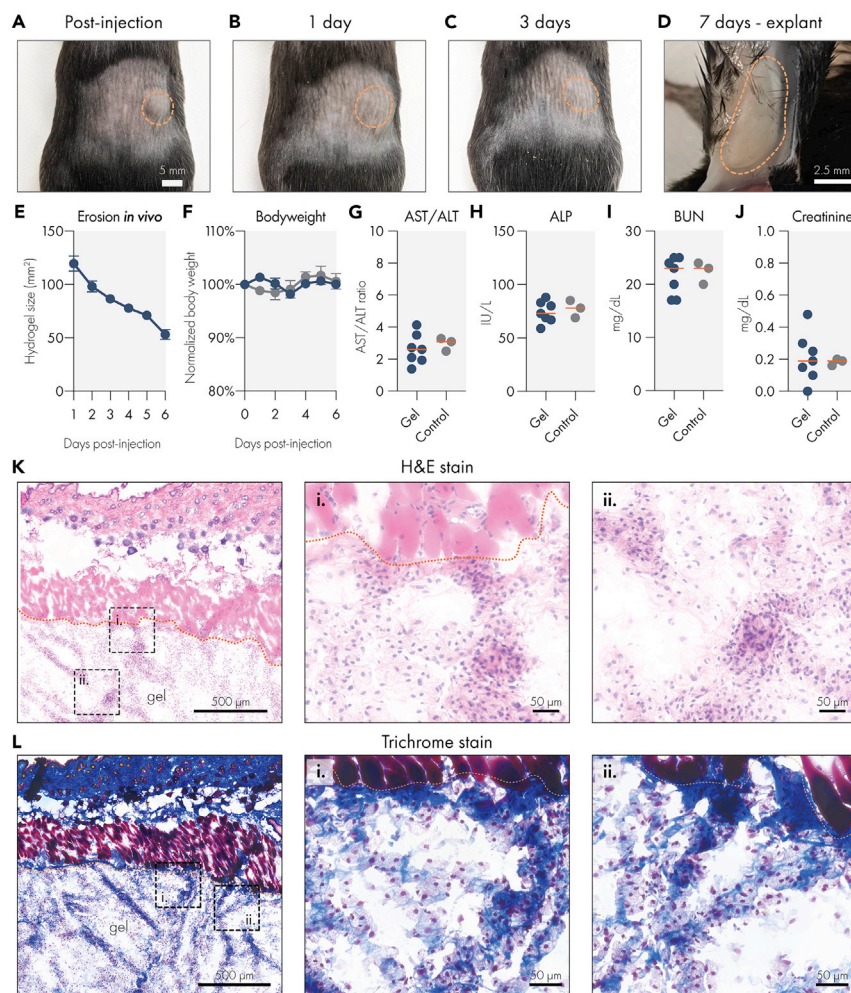
Figure 5. Liposomal hydrogels are biocompatible and biodegradable *in vivo*

Liposomal hydrogels were injected subcutaneously into the flanks of immuno-competent C57BL6 mice.

(A–D) Representative images of hydrogels (A) immediately after injection, (B) 1 day after injection, (C) 3 days after injection, and (D) upon explantation on day 7. Dotted orange line indicates edge of hydrogel depot.

(E) Caliper measurements of hydrogel depot size over time indicate steady erosion of the material *in vivo*. Data points indicate mean and error bars represent SEM.

(F–L) Stable (F) body weights of hydrogel treated mice are consistent with body weights of untreated mice. Data points indicate mean and error bars represent SEM. Blood chemistry panel on serum collected 7 days after hydrogel injection is shown. Liver function was tracked by measuring (G) AST/ALT ratio and (H) ALP levels. Kidney function was tracked by measuring serum (I) BUN and (J) creatinine levels. All blood chemistry measures were consistent between hydrogel treated and untreated control mice. Histological analysis of explanted liposomal hydrogels using (K) H&E or (L) trichrome staining. Scale bars denote 500 µm for leftmost panel and 50 µm for remaining panels.

To determine how the body engages with liposomal hydrogels, we explanted the gels after 7 days and processed them for cryohistology (Figures 5K and 5L). H&E staining of the hydrogel sections revealed robust cellular infiltration into the biomaterial. Interestingly, cellular infiltrates are localized along strands of extracellular matrix (ECM) that are deposited within the hydrogel. In these samples, there is little classical fibrosis along the hydrogel-host interface, and there are no signs of multi-nucleated foreign body giant cells. Overall, these observations indicate that

Matter
Article

CellPress

this material does not evoke a strong foreign body response. Trichrome staining was then used to more closely evaluate the deposition of ECM in and around the hydrogels. This staining method, which renders collagen blue and muscle tissue red, revealed that the strands of tissue deposited into the hydrogel contain abundant collagen. In general, the toxicological and histological data indicate that liposomal hydrogels are well tolerated in the subcutaneous space and that these hydrogels are easily infiltrated by resident cells and, in particular, macrophages. The ability for cells to infiltrate and remodel this biomaterial presents a promising opportunity for engineering specific cellular niches, such as those currently being explored by immunomodulatory biomaterials.[49,50]

Engineering the surface chemistry of liposomal building blocks enables distinct modes of release for protein cargo

Because protein-based therapeutics are becoming increasingly vital to diverse biomedical applications, we investigated strategies that would improve control over the release of proteins from liposomal hydrogels (Figure 6A). Initially, we investigated the effect of molecule size on diffusion within the hydrogel by conducting a fluorescence recovery after photobleaching (FRAP) experiment.[51] In this study, we measured the mobility of fluorescein-labeled dextran molecules ranging from 40 to 2,000 kDa within the LNH system (Figure 6B). The data indicated that molecular weight greatly impacted diffusion (Figure 6C), confirming that the hydrogel mesh has the potential to slowly release high-molecular-weight (~2,000 kDa) therapeutics, which may be useful for the delivery of bulky cargo (e.g., therapeutic biopolymers, such as polyinosinic-polycytidylic acid [poly(I:C)] adjuvants). In the 40–250 kDa size range (equivalent to a hydrodynamic radius between 4.5 and 12 nm, which also encompasses most protein therapeutics), we observed size-dependent release kinetics consistent with passive-release strategies from hydrogel networks.[7] From these FRAP data, we estimate an apparent polymer mesh size of 4.45 nm.[52]

We then explored two affinity-based strategies to regulate the release of protein drugs from these hydrogels by engineering the surface chemistries of our liposomal building blocks. First, we evaluated how electrostatic interactions influenced the release rate of a charged protein cargo (Figure 6Aii). The DMPG phospholipid in our standard liposome formulation confers a net negative charge to these nanoparticles, which can interact with cationic amino acids. While electrostatic interactions have been leveraged in the past for delaying the release of charged proteins,[53–55] these studies often rely on protein cargo that are intrinsically charged under physiological conditions. In this experiment, we instead introduced the common histidine-based tag (his-tag) onto proteins of interest. Because his-tags consist of a repeating stretch of cationic amino acids, we hypothesized that this motif would be sufficient to confer electrostatic interactions between his-tagged proteins and our anionic liposomal hydrogels.

Our *in vitro* release data confirmed that electrostatic engagement of the his-tag significantly reduced the release rate of GFP from the liposomal hydrogel. We observed that 50% of his-GFP cargo released from anionic liposomal hydrogels over 9 days, whereas 50% of wild-type GFP released from the same hydrogel matrix in only 4 days (Figure 6D). We attribute this to the inability of wild-type GFP to form electrostatic interactions with the anionic liposomes in this LNH formulation, whereas his-GFP is able to engage anionic liposomes through the repeating histidine motif. Over the course of the study, this led to significant differences (q = 0.001) in the area under the release time curve (Figure 6E), indicating his-GFP was better retained by the hydrogels. Fitting release data to the Korsmeyer-Peppas
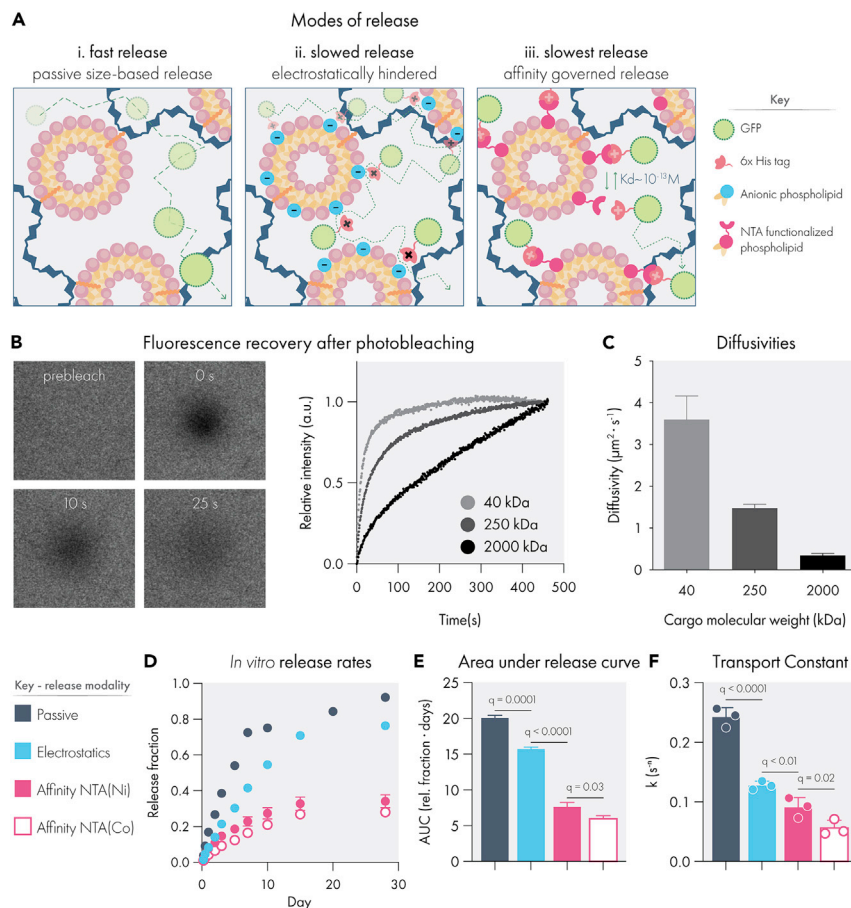
Figure 6. Liposome surface chemistry can be engineered to regulate the release rate of protein cargo

(A) Liposomal hydrogels feature three distinct release modalities based on cargo interaction with liposome surface chemistry.

(B) Representative images and raw data for fluorescence recovery after photo bleaching (FRAP) experiments.

(C) FRAP data were used to calculate size-based diffusivity constants for model cargo (dextran macromolecules) within liposomal hydrogels.

(D) *In vitro* release of his-tagged GFP from liposomal hydrogels engineered to engage the cargo through distinct mechanisms. Samples were maintained at 37°C throughout the study.

(E) Area under the release time curve.

(F) Release data were modeled using the Korsmeyer-Peppas equation to calculate the transport constant.

All data indicate mean and SEM of three independent replicate experiments. Statistical comparisons were made using a one-way ANOVA, and the FDR was controlled at 5% using the Benjamini, Krieger, and Yekutieli method.

model (Figure S7),[56] we estimated a significant 1.9-fold decrease (q < 0.0001) in the transport constant for his-GFP in the anionic liposomal hydrogel compared with wild-type GFP (Figure 6F). These data strongly indicate that engineering electrostatic interactions between the liposomes and protein cargo alter the release mechanism away from a passive, diffusion-based mechanism to one governed by electrostatic affinity. Importantly, this effect was achieved by modifying protein cargo with the his-tag, a common epitope used in purification of recombinant proteins, which extends the utility of electrostatically governed release for many therapeutic proteins. The ability to regulate the release of his-tagged proteins provides a

Matter
Article

CellPress

powerful tool for preclinical studies. Clinical development of the his-tag governed release will need to weigh the benefits of controlled delivery against the potential immunogenicity of retaining affinity tags on proteins of interest. Nevertheless, the clinical value of affinity LNHs could be realized using alternative ligands that recognize native, unmodified protein cargo.

We then set out to determine how specific affinity interactions would further regulate the release rate of protein cargo from this platform. We hypothesized that increasing the affinity for the his-tag motif would substantially slow the release of protein cargo from our material. To this end, we prepared liposomes featuring 3 mol % of either nitrilotriacetic acid (NTA)(Ni)- or NTA(Co)-functionalized phospholipids (Figure 6Aiii). We first confirmed that incorporation of NTA motifs onto the liposomes did not alter the mechanical properties of the resulting hydrogels (Figure S8). These molecular motifs are commonly used in column purification of recombinant proteins, exhibiting extremely high affinity ($K_d \sim 10^{-13}$ M) for the his-tag motif.[57,58] We observed that both NTA(Ni)- and NTA(Co)-functionalized liposomal hydrogels dramatically reduced the release rate of his-GFP *in vitro*, with only 34.1% $\pm$ 0.1% and 28.0% $\pm$ 0.1% of his-GFP released by 30 days, respectively. We noted a slower release rate from NTA(Co) formulations, possibly due to the partial oxidation of Co^{2+} to the Co^{3+} state during synthesis, which has been reported to increase the affinity to his-tag.[59,60] The area under the release curve for NTA-based formulations was significantly reduced (q < 0.0001) compared with both passive and electrostatic release mechanisms. We also noted that NTA(Co) formulations reduced the area under the curve (AUC) compared with NTA(Ni) formulations (q = 0.03).

Consistent with reports that NTA(Co) can exhibit higher affinity for the his-tag motif, the transport constant of his-GFP in NTA(Co) LNH formulations was 38.5% lower than that of NTA(Ni) (q = 0.02; Figure 6F). Impressively, the NTA(Co) affinity-governed release rate is 4.3-fold and 2.3-fold slower than the passive and electrostatic modes of release, respectively. These results are consistent with prior reports leveraging NTA-functionalized phospholipids for tethering proteins onto liposomal drugs, which observed stable loading of his-tagged proteins onto these constructs.[61] While prior studies have focused on the utilization of functionalized liposomes alone for delivery,[62,63] we report the first study to incorporate functionalized liposome as a structural component of an injectable hydrogel depot for applications in extended delivery.

Importantly, these data indicate that, by engineering the surface chemistry of the liposomal building blocks of the LNH system, distinct modes of release can be employed to deliver protein drugs on different timescales. Notably, LNHs release proteins over extremely long timescales compared with previously published reports.[64–66] Of previously reported systems, physical networks functionalized with peptide-binding domains show the most similar sustained release behavior.[67,68] Moreover, as these strategies take advantage of common motifs (e.g., his-tag) used in the production of recombinant proteins, they also allow for orthogonal controlled release of multiple proteins based on the presence or absence of specific molecular handles.

Liposomal hydrogels enable synchronized sustained release of antibodies and cytokines *in vivo*

Because liposomal hydrogels are able to simultaneously mediate orthogonal modes of release, we hypothesized that this biomaterial could be used to synchronize the release kinetics of different sizes and types of protein drugs. With conventional

hydrogels, the release kinetics of multiple co-encapsulated proteins are often dictated by cargo size, with smaller proteins releasing more quickly than larger cargo.[7] The inability to tune relative release rates between cargo is a major limitation for biomaterials, particularly for applications in immuno-engineering and tissue regeneration, where the order of drug presentation can strongly influence outcomes.[3]

To initially test our hypothesis, we modeled hydrogel mediated co-delivery of IgG antibody and the IL-12 cytokine, two important classes of immunotherapy drugs. Because IgG antibodies are relatively bulky (~150 kDa and estimated R_h of ~5.29 nm),[69] we hypothesized that IgG would be effectively retained in our hydrogels using a passive-release mechanism. Using a previously published multiscale model for predicting passive release from hydrogel systems,[52] we estimated the diffusivity of IgG to be 36.9 μm^2/s in a conventional 10 wt % PEG hydrogel.[70] In contrast, we observed a much lower diffusivity (1.3 μm^2/s) of IgG antibody in our LNH system, a roughly 30-fold decrease in IgG diffusivity (Figure S9). This low diffusivity of IgG in the LNH is similar to the predicted self-diffusivity of the polymer mesh of the LNH.[16,42] This observation indicates that the LNH mesh is sufficiently small to constrain IgG diffusion, suggesting that IgG will release for these materials at approximately the rate of LNH erosion. The small LNH mesh is also expected to dramatically reduce the diffusivity of entrapped cytokines. The magnitudes of the diffusivities of both IgG and cytokines are not only much smaller when encapsulated in the LNH than observed in buffer only, but also much more similar to each other, even when no affinity interactions are present (Figure S9).

Overall, our model predicted a highly effective sustained release of IgG from liposomal hydrogels. In contrast, IL-12 is a much smaller protein (~60 kDa and estimated R_h of ~3.18 nm)[69] that we anticipated would be poorly retained using passive release, aligning with our in vitro findings demonstrating rapid passive release of GFP (~40 kDa). To begin evaluating this hypothesis, we modeled the diffusivity of IL-12 in our LNH system, which predicted that, under passive release conditions, IL-12 would diffuse at a rate of 16.5 μm^2/s, which is roughly 13-fold faster diffusivity than IgG. Taken together, our model suggests that purely passive release mechanisms would be incapable of synchronizing the sustained release of these two proteins from a drug delivery vehicle.

To synchronize the release kinetics of these distinctly sized proteins, we leveraged electrostatic interactions to slow the release of IL-12. Interestingly, IL-12 is capable of engaging with charged biomaterials for local drug delivery[71] and engages in electrostatic interactions with densely anionic heparin proteoglycans and endogenous components of the ECM.[72,73] Given these properties, we hypothesized that our LNH system featuring anionic liposomes would be able to dramatically slow the release of IL-12, similar to our in vitro results.

To test this hypothesis, we subcutaneously co-delivered fluorescently labeled IgG and IL-12 proteins in liposomal hydrogels or bolus injections in immuno-competent SKH1E mice (Figure 7A) and analyzed the release of both proteins simultaneously with an in vivo imaging system (IVIS). We selected the 2P-10L formulation for in vivo release studies based on its stronger mechanical properties, which we hypothesized would lead to prolonged depot persistence. Liposome formulation no. 1 (Table S2) was chosen as our base formulation due to its anionic charge and its prior validation as an effective drug carrier.[29] Each protein was labeled with a unique non-overlapping fluorophore to enable simultaneous tracking of both proteins. IVIS imaging revealed that bolus administration led to a rapid decline of both IgG and IL-12 in less
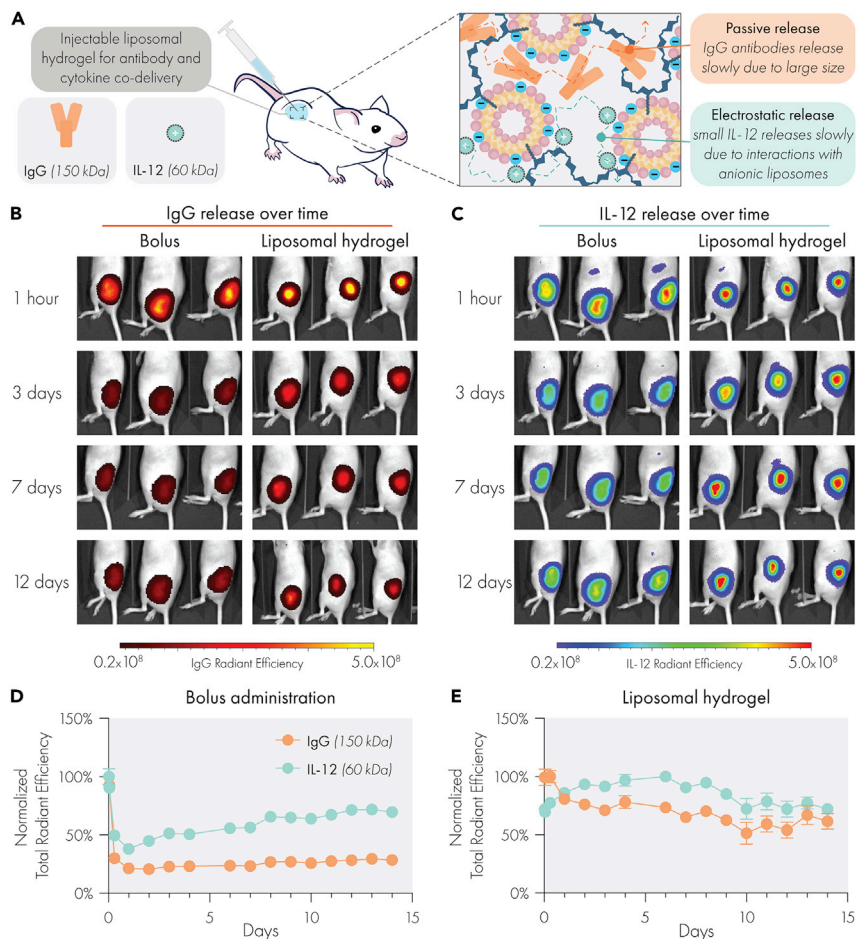
Figure 7. Liposomal hydrogels enable synchronized and sustained co-delivery of IgG antibody and IL-12 cytokine cargo *in vivo*, despite substantial size difference

(A) Liposomal hydrogel mesh size is able to significantly slow release of bulky IgG antibodies, while anionic liposomes regulate release of small IL-12 cytokines via electrostatic interactions.

(B and C) Representative IVIS images of (B) Alexa-Fluor-594-labeled IgG and (C) Alexa-Fluor-700-labeled IL-12 release over time.

(D and E) Quantified release curves of IgG and IL-12 following (D) local subcutaneous bolus injection or (E) subcutaneous injection of liposomal hydrogel. Data points indicate mean and error bars represent SEM. Sample size was n = 3 for bolus and n = 4 for hydrogel groups.

than 1 day. In contrast, liposomal hydrogels closely aligned the release profiles of these two very differently sized proteins. Even after 14 days, the liposomal hydrogels retained over 50% of the fluorescent signal from both proteins.

To demonstrate the ability to tune IL-12 release *in vivo* by engineering the liposome surface chemistry, we also evaluated release of his-tagged IL-12 from NTA(Ni) functionalized LNHs (Figure S10). We observed that IgG release rates were unaffected by changes in liposome surface chemistry, consistent with our hypothesis that these modifications do not interact with antibody cargo. In contrast, we observed a significantly slowed release of IL-12 (compared with the electrostatic affinity system) when using the high-affinity NTA(Ni) LNH formulation.

We note that, in the bolus injections, the release curves plateau, indicating some fraction of cargo is retained in the injection site. We attribute this to immune cells

in the injection site binding the cargo. While we chose isotype IgG and human IL-12 to reduce immuno-activity and simplify pharmacokinetics within this murine model,[74] isotype antibodies still engage Fc receptors on myeloid cells and human IL-12 can still bind to local ECM constituents.[73,75] Similar to our prior fluorescence-based pharmacokinetic studies in hydrogels,[76] we noted a self-quenching phenomenon affecting the IL-12 signal from liposomal hydrogels over our early time points. During this phase, signal increases as fluorescent molecules separate from one another and cease self-quenching.

This study demonstrates the unique capabilities of LNHs to program release of highly physicochemically distinct and translationally relevant molecular cargo *in vivo*. Previously published affinity-based release systems have primarily demonstrated efficacy *in vitro*.[64,65,68] This study is among the first to demonstrate programmable release over uniquely long timescales in a fully immuno-competent *in vivo* setting.

Conclusion

We have developed an injectable liposomal nanocomposite hydrogel biomaterial and demonstrated its exceptional utility in enabling programmable release of diverse protein cargo both *in vitro* and *in vivo*. Comprehensive shear and extensional rheology demonstrate that liposomal hydrogels are highly tunable and modular materials that exhibit gel-like properties, facile injectability, and rapid self-healing ideal for forming drug-releasing depots following administration. Our study reveals that hydrogel formation is highly robust to modifications of the liposomal building blocks, especially with regards to their surface chemistry. In addition, the unique extensibility of these materials showcase promise for applications beyond drug delivery, such as 3D bioprinting or bioadhesives.

To highlight the translational potential of this material, we investigated its biodegradability and biocompatibility in mice through body weight tracking, blood chemistry, and histology. Overall, LNHs eroded gradually *in vivo* and caused no adverse side effects. We also demonstrated multi-modal release mechanisms from the LNH platform that ranged from passive to affinity-based release. FRAP studies indicated that liposomal hydrogels regulate diffusion of bulky protein cargo passively through their small dynamic mesh size. For cargo smaller than the apparent mesh size, we demonstrated two modes of affinity-governed release based on either electrostatic interactions or affinity ligands. In the case of electrostatics, charged liposomes within the LNH system engaged oppositely charged protein cargo. In the case of affinity ligands, NTA-functionalized liposomes within the LNH system selectively bound to his-tagged proteins. In both cases, the release rate of small proteins was reduced to various extents to provide desired release kinetics. Finally, we demonstrated this material's ability to synchronize the delivery of IgG and IL-12, two clinically relevant and differently sized biomolecules, *in vivo*. We found that liposomal hydrogels enabled weeks of sustained, synchronized, and local release of these two distinct protein drugs.

Overall, this report highlights an approach leveraging liposomal nanotechnology to generate a modular, safe, and effective biomaterials platform for coordinating the release kinetics of multiple protein drugs. The ability to inject this material further increases the clinical and translational potential of this technology. These advanced capabilities have impactful implications for a variety of biomedical applications requiring the controlled delivery of multiple drugs, particularly in the areas of tissue and immuno-engineering.

Matter
Article

CellPress

EXPERIMENTAL PROCEDURES

Resource availability

Lead contact

Further information and requests for resources and materials should be directed to and will be fulfilled by the lead contact, Eric A. Appel (eappel@stanford.edu).

Materials availability

This study did not generate new, unique reagents.

Data and code availability

- Data required to evaluate the conclusions of this article are provided within the article and supplemental information. Raw data will be made available from the lead contact upon reasonable request.
- This paper does not report original code; the software used to model diffusion behaviors is publicly available at http://www.supramolecularbiomaterials.com/msdm-calculator, and the software used to model extrudability is publicly available at http://www.supramolecularbiomaterials.com/extrudability.

Materials

All lipids were purchased from Avanti Polar Lipids. See Table S1 for a complete list of lipids and their associated catalog numbers. Hypromellose, N-methylpyrrolidone (NMP), and dodecyl isocyanate were purchased from Sigma-Aldrich. Dialysis tubing was purchased from Spectrum Labs. Sterile PBS was purchased from Thermo Fisher Scientific. Tag-free and histidine-tagged GFP were purchased from MilliporeSigma and Sino Biologicals, respectively. Mouse IgG1 isotype control antibody (clone MOPC-21) was purchased from Bio X Cell. Tag-free and histidine-tagged human IL-12 were both purchased from Sino Biologicals.

Liposome synthesis

Liposomes were prepared via thin-film hydration and extrusion methods. Briefly, the desired amount of phospholipid was dissolved in chloroform or methanol (depending on the solubility of the particular phospholipid) and transferred to a round-bottom flask. The flask was then attached to a Rotary Evaporator (Buchi) and placed under vacuum at 40°C until a thin lipid film was formed. The film was rehydrated in sterile PBS at a concentration ranging from 60 to 150 mg/mL. Rehydration occurred under rotary agitation and at 40°C for 30 min. Following rehydration, the crude liposomal solution was manually extruded through 400, 200, 100, and 50 nm polycarbonate filters (10 passes per each filter) using a hand-extruding device (either Avanti's Mini Extruder or T&T Scientific's NanoSizer MINI system). Size and uniformity of the liposomes were confirmed by dynamic light scattering measurements using the Wyatt DynaPro instrument. Liposomes were used immediately or stored at 4°C until used.

Dodecyl-modified HPMC-C$_{12}$ synthesis

HPMC-C$_{12}$ was prepared as described previously.[24] Briefly, 1 g of hypromellose was dissolved in 40 mL of NMP and heated to 80°C in a PEG bath, with stirring. Dodecyl isocyanate (125 μL) was diluted in 5 mL of NMP and then added dropwise to the hypromellose solution. Hunig's catalyst was added dropwise (10 drops) to the mixture, after which the heat was shut off and the reaction allowed to continue overnight while stirring. The next day, polymer was precipitated in a 600-mL bath of acetone and then dissolved in 40 mL of Millipore water. The dissolved polymer was then purified via dialysis (3.5 kDa molecular weight cutoff [MWCO]) over 4 days at

CellPress

room temperature. Pure HPMC-C_{12} was then lyophilized and dissolved in 1× sterile PBS to yield a 6 wt % solution, which was stored at 4°C until used.

Liposomal hydrogel formation

Hydrogels were formed by simple mixture of liposomes and HPMC-C_{12} either in an Eppendorf tube or using a dual-syringe mixer. In an Eppendorf tube, the desired amount of liposome (measured by volume) and HPMC-C_{12} (measured by weight) were added, with any remaining volume adjustments being made by addition of sterile PBS. A metal spatula was then used to manually mix the solutions until a hydrogel was formed (2 to 3 min). For preparation using the dual-syringe method,[77] the desired amounts of liposome and HPMC-C_{12} solution were loaded into two separate 1-mL luer lock syringes. The two syringes were then securely connected to one another via a luer-lock elbow connector. The solutions were mixed by alternating depression on the connected syringes until the hydrogel formed (determined by an increase in resistance during plunger depression, generally occurring after 100–150 passes). Hydrogel formulations generally consisted of 2 wt % HPMC-C_{12} and varying weight percentages of liposome (either 1%, 4%, or 10%), depending on the particular experimental goals. Formulation shorthand is xP-yL, where x indicates the weight percentage of HPMC-C_{12} and y indicates the weight percentage of liposome. Unless otherwise noted, liposome formulations are 9:1:2 M ratios of DMPC, DMPG, and cholesterol, extruded through 50-nm polycarbonate filters as described above.

Rheological characterization of liposomal hydrogels
Shear rheology

Rheological testing was performed using a 20-mm-diameter serrated parallel plate at a 500-μm gap on a stress-controlled TA Instruments DHR-2 rheometer, unless otherwise specified. All experiments were performed at 25°C. Frequency sweeps were performed at a strain of 1% within the linear viscoelastic regime. Amplitude sweeps were performed at frequency of 10 rads/s. Flow sweeps were performed from high to low shear rates with steady-state sensing. Stress sweeps were performed from low to high with steady-state sensing.

Viscometry

A Rheosense *m*-VROC viscometer was used to measure the hydrogel viscosity at high shear rates from low to high shear rates using a 1 mL Hamilton syringe. Each data point was collected at steady state.

Extensional rheology

Strain-to-break measurements were performed on a TA Instruments ARES-G2 rheometer in axial mode with an 8-mm serrated plate geometry and Hencky strain rates as described by Nelson et al.[48] A serrated parallel plate with a radius of $R_0 = 4$ mm and advanced Peltier system bottom plate were used. Samples containing 400 μL were loaded at a gap of $H_0 = 4$ mm, resulting in an aspect ratio of $\Lambda_0 = H_0/R_0 = 1$. The serrated plate helped to ensure the material would cohesively fail. All experiments were performed at 25°C and replicated three times from independent batches of hydrogel.

Interparticle spacing calculation

The interparticle spacing (IPS) was calculated by the following equation:[30]

$$IPS = 2r\left(\left(\frac{\sigma_m}{\sigma}\right)^{\frac{1}{3}} - 1\right),$$

Matter
Article

CellPress

where σ_m is 0.63, σ is the particle volume fraction, and *r* is the radius of the particle. The number of lipids per liposome was used to calculate the total number of liposomes per volume.

Toxicology studies

All animal studies were performed following Stanford's Institutional Animal Care and Use Committee (IACUC) guidelines and protocols. Biocompatibility was assessed by tracking hydrogel erosion, body weight, and blood chemistry in mice subcutaneously injected with 100 μL of liposomal hydrogel. Mice were injected with hydrogels subcutaneously in the hind flank, and the hydrogel size and mouse weight were tracked daily until the end of the study. During this time, the overall health of the mouse was also evaluated, in particular taking note of any skin irritation or signs of pain and distress (e.g., hunched posture or discontinuation of grooming behaviors). At the end of the study, mice were euthanized and blood collected via cardiac puncture. Blood was processed to recover serum and then submitted to Stanford's Animal Diagnostic Lab for blood work. Hydrogels were also explanted from mice and cryopreserved in OCT compound (Tissue Tek) using liquid nitrogen. Frozen specimens were then submitted to Stanford's Animal Histology Services core facility for sectioning and staining. Stained slides were imaged using a Leica Thunder microscope using a 40× air objective.

Fluorescence recovery after photobleaching experiments

Hydrogels were placed onto glass slides and imaged using a confocal LSM780 microscope at a 20× magnification. Samples were imaged using a low-intensity laser to observe an initial level of fluorescence. Then, the laser was switched to full intensity and focused on a region of interest (ROI) with a 25-μm diameter for 10 s in order to bleach a circular area. Fluorescence data were then recorded for 4 min to create an exponential fluorescence recovery curve. Samples were taken from different regions of each gel (n = 3). The diffusion coefficient was calculated according to

$$D = \gamma_D \left(\omega^2 \,/\, 4\tau_{1/2} \right),$$

where the constant $\gamma_D = \tau_{1/2}/\tau_D$, with $\tau_{1/2}$ being the half-time of the recovery and τ_D the characteristic diffusion time, both yielded by the ZEN software, and ω the radius of the bleached ROI (12.5 μm).[51]

In vitro release studies

Release of GFP from liposomal hydrogels was assessed by plate-reader analysis of serially collected samples as described previously. Briefly, 2P-4L hydrogels were prepared and used to encapsulate 10 μg of recombinant GFP protein (either tag-free or his-tag, depending on the experimental condition). To prepare specimens, approximately 100 μL of hydrogel was injected into the bottom of sealed glass capillary tubes. The remaining volume (200–300 μL) was filled with sterile PBS, and the specimens were then incubated at 37°C in the dark. At the indicated time points, the supernatant was collected and replaced with fresh PBS. The collected supernatants were transferred to a black 96-well plate and analyzed using a plate reader. Three specimens were prepared for each experimental condition.

Fluorescent labeling of proteins

Mouse isotype IgG (Bio X Cell; BE0083, clone MOPC-21) and human IL-12 (Sino Biological; CT011-H08H) were covalently modified with Alexa Fluor dyes using Abcam Lightning Link protein labeling kits according to the manufacturer's instructions. IgG was labeled with Alexa Fluor 598, while IL-12 was labeled with Alexa Fluor 700, two non-overlapping dyes that would enable simultaneous tracking of both cargo with

an IVIS imaging device. After labeling, both proteins were washed and concentrated using VivaSpin 500 desalting columns. Proteins were then mixed with liposomes prior to formation of hydrogels or adjusted to the desired concentration with sterile PBS for bolus administrations.

In vivo release studies

SKH1E nude immuno-competent mice were used to assess the release behavior of LNHs containing labeled IgG and IL-12. Mice were subcutaneously injected in the hind flank with a 100 μL volume of either a bolus solution or a liposomal hydrogel. Each injection administered 10 μg of mouse IgG antibody and 12.5 μg of human IL-12. Isotype control IgG and human IL-12 were chosen for this study because both cargoes were expected to have minimal immuno-activity, which would simplify our experimental system. Mice were imaged sequentially using a PerkinElmer IVIS instrument using automatic exposure acquisition settings. Mice were imaged immediately before injection, 30 min after injection, 1 h after injection, 7 h after injection, and then daily thereafter. Data were analyzed in the LivingImage software. Analysis consisted of defining an ROI over the injection site or hydrogel and exporting the total radiant efficiency measured in that region. Data were normalized to the maximum signal recorded during the study and then plotted in PRISM. Sample was n = 3 for the bolus condition and n = 4 for the liposomal hydrogel condition.

Modeling

To model diffusivity of the IgG and IL-12, the hydrodynamic radius of IgG antibody and IL-12 were assumed to be 5.29 and 3.18 nm, respectively.[69] The dynamic mesh size of the LNH was approximated as 4.452 nm, back calculated using our FRAP diffusivity measurements of dextran molecules of known hydrodynamic radii and utilizing the multiscale diffusion model for solute diffusion in hydrogels calculator derived in Axpe et al.[52,78] Diffusivities of IgG and IL-12 were additionally calculated by the same method in standard PEG hydrogels for comparison by assuming a mesh size of 25 nm and a solid content of 10 wt %.[52]

Statistical methods

Statistical comparisons were made in the GraphPad PRISM statistical software using either a one-way or two-way ANOVA, depending on the nature of the dataset. For all analyses, the false discovery rate was controlled at 5% for multiple comparisons using the Benjamini, Krieger, and Yekutieli method.

SUPPLEMENTAL INFORMATION

Supplemental information can be found online at https://doi.org/10.1016/j.matt.2022.03.001.

AUTHOR CONTRIBUTIONS

Conceptualization, S.C.; methodology, S.C. and A.K.G.; formal analysis, S.C., A.K.G., and H.L.H.; investigation, S.C., A.K.G., and J.H.K.; visualization, S.C.; writing – original draft, S.C. and A.K.G.; writing – review & editing, S.C., A.K.G., J.H.K., and E.A.A.; funding acquisition, S.C., A.K.G., and E.A.A.; supervision, E.A.A.

DECLARATIONS OF INTERESTS

S.C., A.K.G., J.H.K., and E.A.A. are listed as inventors on a patent application reporting the liposomal hydrogel technology described in this article (US patent application no. 63/177,373).

REFERENCES

1. Barrientos, S., Brem, H., Stojadinovic, O., and Tomic-Canic, M. (2014). Clinical application of growth factors and cytokines in wound healing. Wound Repair Regen. 22, 569–578. https://doi.org/10.1111/wrr.12205.

2. Ogay, V., Mun, E.A., Kudaibergen, G., Baidarbekov, M., Kassymbek, K., Zharkinbekov, Z., and Saparov, A. (2020). Progress and prospects of polymer-based drug delivery systems for bone tissue regeneration. Polymers 12, 2881.

3. Schmidt, C. (2017). The benefits of immunotherapy combinations. Nature 552, S67.

4. Yang, B.A., Westerhof, T.M., Sabin, K., Merajver, S.D., and Aguilar, C.A. (2021). Engineered tools to study intercellular communication. Adv. Sci. 8, 2002825. https://doi.org/10.1002/advs.202002825.

5. Gupta, K.K., Khan, M.A., and Singh, S.K. (2020). Constitutive inflammatory cytokine storm: a major threat to human health. J. Interferon Cytokine Res. 40, 19–23.

6. Roth, G.A., Picece, V.C., Ou, B.S., Luo, W., Pulendran, B., and Appel, E.A. (2021). Designing spatial and temporal control of vaccine responses. Nat. Rev. Mater. 7, 1–22.

7. Correa, S., Grosskopf, A.K., Lopez Hernandez, H., Chan, D., Yu, A.C., Stapleton, L.M., and Appel, E.A. (2021). Translational applications of hydrogels. Chem. Rev. 121, 11385–11457.

8. Correa, S., Dreaden, E.C., Gu, L., and Hammond, P.T. (2016). Engineering nanolayered particles for modular drug delivery. J. Control. Release 240, 364–386.

9. Manzoor, A.A., Lindner, L.H., Landon, C.D., Park, J.-Y., Simnick, A.J., Dreher, M.R., Das, S., Hanna, G., Park, W., and Chilkoti, A. (2012). Overcoming limitations in nanoparticle drug delivery: triggered, intravascular release to improve drug penetration into tumors. Cancer Res. 72, 5566–5575.

10. Zhang, L., Gu, F., Chan, J., Wang, A., Langer, R., and Farokhzad, O. (2008). Nanoparticles in medicine: therapeutic applications and developments. Clin. Pharmacol. Ther. 83, 761–769.

11. Wilhelm, S., Tavares, A.J., Dai, Q., Ohta, S., Audet, J., Dvorak, H.F., and Chan, W.C.W. (2016). Analysis of nanoparticle delivery to tumours. Nat. Rev. Mater. 1, 16014. https://doi.org/10.1038/natrevmats.2016.14.

12. Varanko, A., Saha, S., and Chilkoti, A. (2020). Recent trends in protein and peptide-based biomaterials for advanced drug delivery. Adv. Drug Deliv. Rev. 156, 133.

13. Tous, E., Purcell, B., Ifkovits, J.L., and Burdick, J.A. (2011). Injectable acellular hydrogels for cardiac repair. J. Cardiovasc. Trans. Res. 4, 528–542.

14. Tong, X., and Yang, F. (2016). Sliding hydrogels with mobile molecular ligands and crosslinks as 3D stem cell niche. Adv. Mater. 28, 7257–7263.

15. Tysseling, V.M., Sahni, V., Pashuck, E.T., Birch, D., Hebert, A., Czeisler, C., Stupp, S.I., and Kessler, J.A. (2010). Self-assembling peptide amphiphile promotes plasticity of serotonergic fibers following spinal cord injury. J. Neurosci. Res. 88, 3161–3170.

16. Roth, G.A., Gale, E.C., Alcántara-Hernández, M., Luo, W., Axpe, E., Verma, R., Yin, Q., Yu, A.C., Lopez Hernandez, H., Maikawa, C.L., et al. (2020). Injectable hydrogels for sustained codelivery of subunit vaccines enhance humoral immunity. ACS Cent. Sci. 6, 1800–1812.

17. Grosskopf, A.K., Roth, G.A., Smith, A.A.A., Gale, E.C., Hernandez, H.L., and Appel, E.A. (2020). Injectable supramolecular polymer-nanoparticle hydrogels enhance human mesenchymal stem cell delivery. Bioeng. Transl. Med. 5, e10147. https://doi.org/10.1002/btm2.10147.

18. Correa, S., Gale, E.C., Mayer, A.T., Xiao, Z., Liong, C., Klich, J.H., Brown, R.A., Meany, E., Saouaf, O., Maikawa, C.L., et al. (2021). Injectable nanoparticle-based hydrogels enable the safe and effective deployment of immunostimulatory CD40 agonist antibodies. Preprint at bioRxiv. https://doi.org/10.1101/2021.06.27.449987.

19. Mann, J.L., Yu, A.C., Agmon, G., and Appel, E.A. (2018). Supramolecular polymeric biomaterials. Biomater. Sci. 6, 10–37.

20. Webber, M.J., Appel, E.A., Meijer, E., and Langer, R. (2016). Supramolecular biomaterials. Nat. Mater. 15, 13–26.

21. Gale, E.C., Powell, A.E., Roth, G.A., Meany, E.L., Yan, J., Ou, B.S., Grosskopf, A.K., Adamska, J., Picece, V.C.T.M., d'Aquino, A.I., et al. (2021). Hydrogel-based slow release of a receptor-binding domain subunit vaccine elicits neutralizing antibody responses against SARS-CoV-2. Adv. Mater. 33, 2104362.

22. Appel, E.A., del Barrio, J., Loh, X.J., and Scherman, O.A. (2012). Supramolecular polymeric hydrogels. Chem. Soc. Rev. 41, 6195–6214.

23. Bernhard, S., and Tibbitt, M.W. (2021). Supramolecular engineering of hydrogels for drug delivery. Adv. Drug Deliv. Rev. 171, 240–256.

24. Appel, E.A., Tibbitt, M.W., Webber, M.J., Mattix, B.A., Veiseh, O., and Langer, R. (2015). Self-assembled hydrogels utilizing polymer–nanoparticle interactions. Nat. Commun. 6, 6295.

25. Meis, C.M., Grosskopf, A.K., Correa, S., and Appel, E.A. (2021). Injectable supramolecular polymer-nanoparticle hydrogels for cell and drug delivery applications. JoVE, e62234. https://doi.org/10.3791/62234.

26. Anthony, C.Y., Lian, H., Kong, X., Hernandez, H.L., Qin, J., and Appel, E.A. (2021). Physical networks from entropy-driven non-covalent interactions. Nat. Commun. 12, 1–9.

27. Allen, T.M., Sapra, P., and Moase, E. (2002). Use of the post-insertion method for the formation of ligand-coupled liposomes. Cell. Mol. Biol. Lett. 7, 217–219.

28. Steele, A.N., Stapleton, L.M., Farry, J.M., Lucian, H.J., Paulsen, M.J., Eskandari, A., Hironaka, C.E., Thakore, A.D., Wang, H., and

Yu, A.C. (2019). A biocompatible therapeutic catheter-deliverable hydrogel for in situ tissue engineering. Adv. Healthc. Mater. *8*, 1801147.

29. Immordino, M.L., Brusa, P., Arpicco, S., Stella, B., Dosio, F., and Cattel, L. (2003). Preparation, characterization, cytotoxicity and pharmacokinetics of liposomes containing docetaxel. J. Control. Release *91*, 417–429.

30. Hao, T., and Riman, R.E. (2006). Calculation of interparticle spacing in colloidal systems. J. Colloid Interf. Sci. *297*, 374–377.

31. Rao, Z., Inoue, M., Matsuda, M., and Taguchi, T. (2011). Quick self-healing and thermo-reversible liposome gel. Colloids Surf. B *82*, 196–202.

32. Lopez Hernandez, H., Souza, J.W., and Appel, E.A. (2021). A quantitative description for designing the extrudability of shear-thinning physical hydrogels. Macromol. Biosci. *21*, 2000295.

33. Li, L., Yan, B., Yang, J., Chen, L., and Zeng, H. (2015). Novel mussel-inspired injectable self-healing hydrogel with anti-biofouling property. Adv. Mater. *27*, 1294–1299.

34. Felgner, J.H., Kumar, R., Sridhar, C., Wheeler, C.J., Tsai, Y.J., Border, R., Ramsey, P., Martin, M., and Felgner, P.L. (1994). Enhanced gene delivery and mechanism studies with a novel series of cationic lipid formulations. J. Biol. Chem. *269*, 2550–2561.

35. Ding, X., Yang, C., Lim, T.P., Hsu, L.Y., Engler, A.C., Hedrick, J.L., and Yang, Y.-Y. (2012). Antibacterial and antifouling catheter coatings using surface grafted PEG-b-cationic polycarbonate diblock copolymers. Biomaterials *33*, 6593–6603.

36. Briuglia, M.-L., Rotella, C., McFarlane, A., and Lamprou, D.A. (2015). Influence of cholesterol on liposome stability and on in vitro drug release. Drug Deliv. Trans. Res. *5*, 231–242.

37. Roy, B., Guha, P., Bhattarai, R., Nahak, P., Karmakar, G., Chettri, P., and Panda, A.K. (2016). Influence of lipid composition, pH, and temperature on physicochemical properties of liposomes with curcumin as model drug. J. Oleo Sci. *65*, 399–411.

38. Stapleton, L.M., Steele, A.N., Wang, H., Hernandez, H.L., Anthony, C.Y., Paulsen, M.J., Smith, A.A., Roth, G.A., Thakore, A.D., and Lucian, H.J. (2019). Use of a supramolecular polymeric hydrogel as an effective post-operative pericardial adhesion barrier. Nat. Biomed. Eng. *3*, 611–620.

39. Osório, L.A., Silva, E., and Mackay, R.E. (2021). A Review of biomaterials and scaffold fabrication for organ-on-a-chip (OOAC) systems. Bioengineering *8*, 113.

40. Chaudhuri, O. (2017). Viscoelastic hydrogels for 3D cell culture. Biomater. Sci. *5*, 1480–1490.

41. Jin, W., Tamzalit, F., Chaudhuri, P.K., Black, C.T., Huse, M., and Kam, L.C. (2019). T cell activation and immune synapse organization respond to the microscale mechanics of structured surfaces. Proc. Natl. Acad. Sci. *116*, 19835–19840.

42. Grosskopf, A.K., Saouaf, O.A., Lopez Hernandez, H., and Appel, E.A. (2021). Gelation and yielding behavior of polymer–nanoparticle hydrogels. J. Poly. Sci. *59*, 2854–2866.

43. Anthony, C.Y., Smith, A.A., and Appel, E.A. (2020). Structural considerations for physical hydrogels based on polymer–nanoparticle interactions. Mol. Syst. Des. Eng. *5*, 401–407.

44. Aguado, B.A., Mulyasasmita, W., Su, J., Lampe, K.J., and Heilshorn, S.C. (2012). Improving viability of stem cells during syringe needle flow through the design of hydrogel cell carriers. Tissue Eng. Part A *18*, 806–815. https://doi.org/10.1089/ten.TEA.2011.0391.

45. Lauser, K.T., Rueter, A.L., and Calabrese, M.A. (2021). Small-volume extensional rheology of concentrated protein and protein-excipient solutions. Soft Matter *17*, 9624–9635.

46. Tang, J.D., Roloson, E.B., Amelung, C.D., and Lampe, K.J. (2019). Rapidly assembling pentapeptides for injectable delivery (RAPID) hydrogels as cytoprotective cell carriers. ACS Biomater. Sci. Eng. *5*, 2117–2121.

47. Rauzan, B.M., Nelson, A.Z., Lehman, S.E., Ewoldt, R.H., and Nuzzo, R.G. (2018). Particle-free emulsions for 3D printing elastomers. Adv. Funct. Mater. *28*, 1707032.

48. Nelson, A.Z., and Ewoldt, R.H. (2017). Design of yield-stress fluids: a rheology-to-structure inverse problem. Soft Matter *13*, 7578–7594.

49. Weiden, J., Voerman, D., Dölen, Y., Das, R.K., Van Duffelen, A., Hammink, R., Eggermont, L.J., Rowan, A.E., Tel, J., and Figdor, C.G. (2018). Injectable biomimetic hydrogels as tools for efficient T cell expansion and delivery. Front. Immunol. *9*, 2798.

50. Adu-Berchie, K., and Mooney, D.J. (2020). Biomaterials as local niches for immunomodulation. Acc. Chem. Res. *53*, 1749–1760. https://doi.org/10.1021/acs.accounts.0c00341.

51. Axelrod, D., Koppel, D., Schlessinger, J., Elson, E., and Webb, W.W. (1976). Mobility measurement by analysis of fluorescence photobleaching recovery kinetics. Biophys. J. *16*, 1055–1069.

52. Axpe, E., Chan, D., Offeddu, G.S., Chang, Y., Merida, D., Hernandez, H.L., and Appel, E.A. (2019). A multiscale model for solute diffusion in hydrogels. Macromolecules *52*, 6889–6897.

53. Nakamae, K., Nizuka, T., Miyata, T., Furukawa, M., Nishino, T., Kato, K., Inoue, T., Hoffman, A.S., and Kanzaki, Y. (1997). Lysozyme loading and release from hydrogels carrying pendant phosphate groups. J. Biomater. Sci. Polym. Ed. *9*, 43–53. https://doi.org/10.1163/156856297x00254.

54. Lee, F., Chung, J.E., and Kurisawa, M. (2009). An injectable hyaluronic acid–tyramine hydrogel system for protein delivery. J. Control. Release *134*, 186–193. https://doi.org/10.1016/j.jconrel.2008.11.028.

55. Huynh, D.P., Nguyen, M.K., Pi, B.S., Kim, M.S., Chae, S.Y., Lee, K.C., Kim, B.S., Kim, S.W., and Lee, D.S. (2008). Functionalized injectable hydrogels for controlled insulin delivery. Biomaterials *29*, 2527–2534. https://doi.org/10.1016/j.biomaterials.2008.02.016.

56. Wu, I.Y., Bala, S., Škalko-Basnet, N., and Di Cagno, M.P. (2019). Interpreting non-linear drug diffusion data: utilizing Korsmeyer-Peppas model to study drug release from liposomes. Eur. J. Pharm. Sci. *138*, 105026.

57. Schmitt, J., Hess, H., and Stunnenberg, H.G. (1993). Affinity purification of histidine-tagged proteins. Mol. Biol. Rep. *18*, 223–230. https://doi.org/10.1007/BF01674434.

58. Bornhorst, J.A., and Falke, J.J. (2000). Purification of proteins using polyhistidine affinity tags. Methods Enzymol. *326*, 245–254. https://doi.org/10.1016/s0076-6879(00)26058-8.

59. Wegner, S.V., and Spatz, J.P. (2013). Cobalt (III) as a stable and inert mediator ion between NTA and His6-tagged proteins. Angew. Chem. Int. Ed. *52*, 7593–7596.

60. Wegner, S.V., Schenk, F.C., and Spatz, J.P. (2016). Cobalt (III)-Mediated permanent and stable immobilization of histidine-tagged proteins on NTA-functionalized surfaces. Chem. Eur. J. *22*, 3156–3162.

61. Colletier, J.-P., Chaize, B., Winterhalter, M., and Fournier, D. (2002). Protein encapsulation in liposomes: efficiency depends on interactions between protein and phospholipid bilayer. BMC Biotechnol. *2*, 1–8.

62. Shao, S., Geng, J., Yi, H.A., Gogia, S., Neelamegham, S., Jacobs, A., and Lovell, J.F. (2015). Functionalization of cobalt porphyrin–phospholipid bilayers with his-tagged ligands and antigens. Nat. Chem. *7*, 438–446.

63. Barberio, A.E., Smith, S.G., Correa, S., Nguyen, C., Nhan, B., Melo, M., Tokatlian, T., Suh, H., Irvine, D.J., and Hammond, P.T. (2020). Cancer cell coating nanoparticles for optimal tumor-specific cytokine delivery. ACS Nano *14*, 11238–11253. https://doi.org/10.1021/acsnano.0c03109.

64. Lin, C.C., and Metters, A.T. (2007). Metal-chelating affinity hydrogels for sustained protein release. J. Biomed. Mater. Res. Part A *83*, 954–964.

65. Lin, C.-C., and Metters, A.T. (2008). Bifunctional monolithic affinity hydrogels for dual-protein delivery. Biomacromolecules *9*, 789–795.

66. Huang, J.-F., Zhong, J., Chen, G.-P., Lin, Z.-T., Deng, Y., Liu, Y.-L., Cao, P.-Y., Wang, B., Wei, Y., and Wu, T. (2016). A hydrogel-based hybrid theranostic contact lens for fungal keratitis. ACS Nano *10*, 6464–6473.

67. Vulic, K., and Shoichet, M.S. (2012). Tunable growth factor delivery from injectable hydrogels for tissue engineering. J. Am. Chem. Soc. *134*, 882–885. https://doi.org/10.1021/ja210638x.

68. Vulic, K., and Shoichet, M.S. (2014). Affinity-based drug delivery systems for tissue repair and regeneration. Biomacromolecules *15*, 3867–3880.

69. Armstrong, J.K., Wenby, R.B., Meiselman, H.J., and Fisher, T.C. (2004). The hydrodynamic radii of macromolecules and their effect on red blood cell aggregation. Biophys. J. *87*, 4259–4270.

Matter
Article

CellPress

70. Offeddu, G., Axpe, E., Harley, B., and Oyen, M. (2018). Relationship between permeability and diffusivity in polyethylene glycol hydrogels. AIP Adv. 8, 105006.

71. Ishii, S., Kaneko, J., and Nagasaki, Y. (2016). Development of a long-acting, protein-loaded, redox-active, injectable gel formed by a polyion complex for local protein therapeutics. Biomaterials 84, 210–218.

72. Jayanthi, S., Koppolu, B.p., Nguyen, K.G., Smith, S.G., Felber, B.K., Kumar, T.K.S., and Zaharoff, D.A. (2017). Modulation of Interleukin-12 activity in the presence of heparin. Sci. Rep. 7, 5360. https://doi.org/10.1038/s41598-017-05382-1.

73. Nguyen, K.G., Gillam, F.B., Hopkins, J.J., Jayanthi, S., Gundampati, R.K., Su, G., Bear, J., Pilkington, G.R., Jalah, R., and Felber, B.K. (2019). Molecular mechanisms of heparin-induced modulation of human interleukin 12 bioactivity. J. Bio. Chem. 294, 4412–4424.

74. Cho, D., Lee, W.J., Halloran, P.J., Trinchieri, G., and Kim, Y.B. (1996). Enhancement of porcine natural killer cell activity by recombinant human and murine IL-12. Cell. Immunol. 172, 29–34. https://doi.org/10.1006/cimm.1996.0211.

75. Weinshank, R.L., Luster, A.D., and Ravetch, J.V. (1988). Function and regulation of a murine macrophage-specific IgG Fc receptor, Fc gamma R-alpha. J. Exp. Med. 167, 1909–1925. https://doi.org/10.1084/jem.167.6.1909.

76. Rao, J., Dragulescu-Andrasi, A., and Yao, H. (2007). Fluorescence imaging in vivo: recent advances. Curr. Opin. Biotechnol. 18, 17–25.

77. Wisdom, K., and Chaudhuri, O. (2017). 3D cell culture in interpenetrating networks of alginate and rBM matrix. In 3D Cell Culture: Methods and Protocols, Z. Koledova, ed. (Springer New York), pp. 29–37. https://doi.org/10.1007/978-1-4939-7021-6_3.

78. Saouaf, O.M., Roth, G.A., Ou, B.S., Smith, A.A., Yu, A.C., Gale, E.C., Grosskopf, A.K., Picece, V.C., and Appel, E.A. (2021). Modulation of injectable hydrogel properties for slow co-delivery of influenza subunit vaccine components enhance the potency of humoral immunity. J. Biomed. Mater. Res. Part A 109, 2173–2186. https://doi.org/10.1002/jbm.a.37203.